

NUMERICAL INVESTIGATION ON INTERACTION BETWEEN A SEMI-SUBMERSIBLE PLATFORM AND ITS MOORING SYSTEM

Yuanchuan Liu

School of Naval Architecture,
Ocean and Civil Engineering,
State Key Laboratory of Ocean
Engineering, Shanghai Jiao
Tong University
Shanghai, China

Yao Peng

School of Naval Architecture,
Ocean and Civil Engineering,
State Key Laboratory of Ocean
Engineering, Shanghai Jiao
Tong University, Collaborative
Innovation Center for Advanced
Ship and Deep-Sea Exploration
Shanghai, China

Decheng Wan

School of Naval Architecture,
Ocean and Civil Engineering,
State Key Laboratory of Ocean
Engineering, Shanghai Jiao
Tong University, Collaborative
Innovation Center for Advanced
Ship and Deep-Sea Exploration
Shanghai, China
Corresponding author
Email: dcwan@sjtu.edu.cn

ABSTRACT

With the increasing demand of floating structures in offshore, coastal and marine renewable energy engineering, the interaction between the mooring system and floating structure becomes more and more important. In this paper, motion responses of a semi-submersible platform with mooring system under regular wave conditions are investigated numerically by a viscous flow solver naoe-FOAM-SJTU based on the open source toolbox OpenFOAM. Influence of the mooring system on the platform motion responses is evaluated in two different ways. Investigations are covered for analysis methods adopted for solving mooring lines and the length of each part of a multi-component mooring line. Several important conclusions are drawn.

Keywords: Motion response, semi-submersible platform, mooring system, naoe-FOAM-SJTU solver.

INTRODUCTION

Traditionally, floating structures are commonly used as equipment for the exploration/exploitation of deep-water oil and gas, such as semi-submersible platforms, Spars and Tension Leg Platforms (TLP). In recent years, with the development of offshore wind turbines in deep water (>30m), adopting floating platforms to support such wind turbine is becoming a new trend to decreasing the economic cost. Unlike their counterparts with fixed bottoms, these floating structures need be equipped with essential mooring systems to resist the motion responses induced by environmental loads from continuous wind, wave and current at sea. The investigation of mooring systems,

especially their effects on the moored structures, thus, has great significance for the design of floating structures.

Over the past few years, a lot of research has been done covering the effect of mooring system on floating structure in different aspects. Some research is focused on the development of various modeling methods. Tahar and Kim (2008) built a time domain coupled analysis tool to study a deep-water floating platform with polyester mooring lines. The rod theory and finite element method (FEM) were adopted for solving mooring lines, taking into account the large elongation and nonlinear stress-strain relationships of lines. Their numerical investigations showed that the inclusion of these parameters could produce more stable and reliable results for high strain cases and influence platform motion as well as line tension. Waris and Ishihara (2010, 2012) investigated the applicability of linear and nonlinear FEM mooring models to both tension leg mooring and catenary mooring systems for a floating offshore wind turbine system. Results showed a good agreement between linear and nonlinear models for tension leg mooring while surge response was overestimated by the linear model for the catenary mooring system. Hall, et al. (2011) studied the effects of two different mooring models (i.e. a fully FEM-based mooring model and a quasi-static catenary model) on the dynamic response of a spar-buoy floating wind turbine OC3-Hywind. Only minor difference is observed in the results obtained under regular wave conditions. Recent study of Sethuraman and Venugopal (2013) revealed that an accurate modeling of mooring line dynamics must consider the structure non-linearity and damping. This was based on their examination for coupled hydrodynamic response of a 1:100

scale model of a floating stepped-spar wind turbine under regular and irregular wave conditions. Using two methods for mooring lines, i.e. linear spring method and nonlinear FEM, Kim, et al. (2013) compared the dynamic coupled behavior of moored floating structures in time domain. It was found that the transient motion response of structures was influenced by the adoption of FEM which takes mooring damping into account.

Apart from modeling methods, effects of various mooring system configurations on the motion response of platform are also partially covered. These include the mooring line number, length and position. For example, using a non-linear analysis tool Yilmaz and Incecik (1996) studied the dynamic motion response of a tanker and the mooring force for a single point moored tanker-buoy system by reducing the number of mooring lines from eight to four. Results showed increased motion response of both the tanker and the buoy as well as enlarged tension in the hawser, which is attributed to the sudden acceleration of the buoy and/or the tanker. Diamantoulaki and Angelides (2011) carried out a parametric study of mooring line number's influence on the performance of a cable-moored array of floating breakwaters. The study is based on a frequency domain method under the monochromatic linear wave conditions. Increasing line number was found to exert little influence on the heave motion of breakwaters. Sun, et al. (2012) investigated the performance of a moored Spar platform and its mooring system under three different mooring configurations using a 3D hydrodynamic finite element model. Jeon, et al. (2013) studied the dynamic response of a floating substructure of a rigid spar-type offshore wind turbine with catenary mooring cables. In their study, the length and connection point of mooring cables were varied. The upper part of wind turbine was modeled as a lumped mass for simplification and coupled BEM-FEM methods were adopted to simulate wave-floating substructure and wave-mooring cable interactions. Their results showed that increasing cable length decreased peak amplitudes in surge and pitch motion responses, and the responses were minimized when mooring cables were connected to or slightly above the center of buoyancy.

Obviously, various mooring types also play significant roles on the motion response of floating platforms. Rahman, et al. (2006) studied the nonlinear dynamics of a pontoon type submerged floating breakwater in regular waves and the mooring line forces for both vertical and inclined mooring systems. The Volume of Fluid (VOF) method combined with the porous body model was adopted to simulate wave-body interaction. Seebai and Sundaravadivelu (2009) experimentally investigated the behavior of a spar platform for a 5MW floating offshore wind turbine with taut and catenary mooring systems. The taut moored model showed smaller responses of both surge and heave than the catenary moored model. Qiao and Ou (2013) performed their study with three types of mooring systems, i.e. catenary, semi-taut and taut, of a semi-submersible platform using a 3D hydrodynamic finite element model. Natural periods, damping ratios, motion responses of the platform and mooring line tensions were compared.

Most of the above mentioned work on moored floating structures utilizes potential flow theory in either frequency or time domain to deal with the fluid-structure interaction problems because of short computing time and good accuracy. However, when it comes to the problems with strong nonlinear phenomena, such as green water, slamming and vortex induced vibration (VIV) of Spars, the traditional theory has its limitations to accurately predict the dynamic response. Computational Fluid Dynamics (CFD) methods might be employed to obtain a better result via employing a more realistic model. In this paper, a *viscous* flow solver (naoe-FOAM-SJTU) (Shen and Wan, 2013; Zhou and Wan, 2013; Cao and Wan, 2014; Zha and Wan, 2014; Zhao and Wan, 2015) which is developed and based on the popular open source toolbox OpenFOAM for predicting dynamics of floating structures with mooring systems is presented. The solver is adopted to study motion responses of a floating semi-submersible platform with a catenary mooring system under regular wave conditions. The study is also extended to the mooring loading. The outline of this paper is as follows. Mathematical equations and numerical methods are first described concerning fluid flow, floating structures and mooring systems. Parameters of the platform and mooring system studied here together with computational domain are then presented. Validations are carried out subsequently to justify the correctness of numerical simulation. Effects of the mooring system are assessed by comparing platform response, mooring system horizontal restoring force, and mooring line tension between static and dynamic methods employed for solving mooring lines. Various configurations with different mooring line composition are also examined. Discussions and conclusions are made at the end.

MATHEMATICAL EQUATIONS

The present solver naoe-FOAM-SJTU adopted for numerical simulation is based on a built-in solver in OpenFOAM named interDyMfoam, which can be used to solve two incompressible, isothermal immiscible fluids with dynamic mesh motion. To deal with common fluid-structure interaction problems in ship hydrodynamics and offshore engineering, several modules are further developed and integrated into the solver, such as a wave generation/damping module, a six-degrees-of-freedom (6DoF) module and a mooring system module. Mathematical formulae related to the solver are described as follows in detail.

1. Governing equations

For transient, incompressible and viscous fluid, flow problems are governed by Navier-Stokes equations:

$$\nabla \cdot \mathbf{U} = 0 \quad (1)$$

$$\frac{\partial \rho \mathbf{U}}{\partial t} + \nabla \cdot (\rho (\mathbf{U} - \mathbf{U}_g) \mathbf{U}) = -\nabla p_d - \mathbf{g} \cdot \mathbf{x} \nabla \rho + \nabla \cdot (\mu \nabla \mathbf{U}) + \mathbf{f}_\sigma \quad (2)$$

where \mathbf{U} and \mathbf{U}_g represent velocity of flow field and grid nodes separately; $p_d = p - \rho \mathbf{g} \cdot \mathbf{x}$ is dynamic pressure

of flow field by subtracting the hydrostatic part from total pressure p ; \mathbf{g} , ρ and μ denote the gravity acceleration vector, density and dynamic viscosity of fluid respectively; \mathbf{f}_σ is surface tension which only takes effect at the free surface and equals zero elsewhere.

2. Free surface capturing

To solve problems related to a floating platform, how to cope with air-water interface becomes of great significance. Volume of Fluid (VOF) method (Hirt and Nichols, 1981) is adopted in OpenFOAM to capture free surface.

Volume fraction function denoted as α is defined for every cell, representing the ratio of cell volume fluid occupies. Therefore, this function α follows the distribution below:

$$\begin{cases} \alpha = 0, & \text{air} \\ \alpha = 1, & \text{water} \\ 0 < \alpha < 1, & \text{free surface} \end{cases} \quad (3)$$

The volume fraction function α is governed by the following transport equation:

$$\frac{\partial \alpha}{\partial t} + \nabla \cdot [(\mathbf{U} - \mathbf{U}_g)\alpha] + \nabla \cdot [\mathbf{U}_r(1-\alpha)\alpha] = 0 \quad (4)$$

To better capture free surface, a bounded compression technique (Rusche, 2002) is adopted which introduces an additional compression term on the left-hand side of equation (4), where \mathbf{U}_r is a relative velocity field. The compression term only functions near free surface due to $(1-\alpha)\alpha$. During the procedure, equation (4) is solved to obtain volume fraction of each cell and free surface is then determined.

For two-phase flow problems, the physical properties of one fluid are calculated as weighted averages based on volume fraction of water and air in one cell as follows:

$$\begin{cases} \rho = \alpha\rho_l + (1-\alpha)\rho_g \\ \mu = \alpha\mu_l + (1-\alpha)\mu_g \end{cases} \quad (5)$$

Where subscripts l and g denote liquid and gas separately.

3. Wave generation

For floating structures, wave loading must be considered to calculate motion response of structures. Wave generation thus must be implemented numerically. The present solver incorporates a wave generation module which can model various types of wave such as linear waves, Stokes 2nd order waves, freak waves, solitary waves, etc. Wave is generated by specifying free surface and velocity distribution at inlet boundary with various wave theories (Baudic, et al., 2001). This method effectively avoids the movement of the boundary and is able to model short-crested irregular waves in the meanwhile through similar configurations at two adjacent boundaries.

The linear wave theory is adopted in this paper and the equation used to describe free surface is:

$$\eta = A \cos \theta \quad (6)$$

The horizontal and vertical components of fluid velocity distribution are shown in the equations below:

$$\begin{cases} u = \frac{\pi H}{T} \frac{\cosh k(z+d)}{\sinh kd} \sin \theta \\ w = \frac{\pi H}{T} \frac{\sinh k(z+d)}{\sinh kd} \cos \theta \end{cases} \quad (7)$$

Where A and $H = 2A$ denote wave amplitude and wave height; T , k , d , $\theta = kx - \omega t$ and ω represent wave period, wave number, water depth, phase and wave frequency respectively.

4. Wave damping

In general, reflection often occurs when wave propagates towards outlet boundary owing to inefficient wave transmission through the boundary. Reflected wave travels in a direction opposite to the incident wave, and thus interferes with each other, influencing the wave pattern. A wave damping module is therefore developed in the present solver, which sets up a wave damping zone, i.e. sponge layer (Larsen and Dancy, 1983), near the outlet boundary to alleviate wave reflection.

Sponge layer takes effect by adding an additional artificial viscous term to the source term of the momentum equation. The new term is expressed as:

$$\mathbf{f}_s = -\rho\mu_s\mathbf{U} \quad (8)$$

Where μ_s is the artificial viscosity calculated by the following equation:

$$\mu_s(x) = \begin{cases} \alpha_s \left(\frac{x-x_0}{L_s} \right)^2, & x > x_0 \\ 0, & x \leq x_0 \end{cases} \quad (9)$$

Where α_s is a dimensionless quantity defining damping strength for the sponge layer. Other variables are explained in Figure 1: x denotes the coordinates in x direction of grid cells; x_0 and L_s represent the position and length of the sponge layer. The artificial viscous term is only effective for cells belonging to the sponge layer and is equal to zero elsewhere. It is worth mentioning that a similar wave damping zone can be easily configured in the y direction.

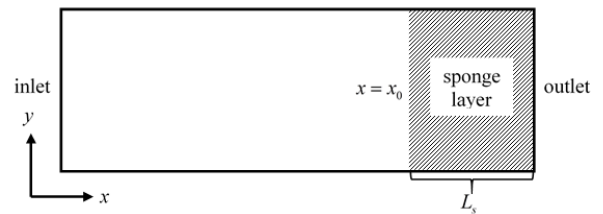


Figure 1 Sketch of sponge layer

5. Motion equations

Excited by environmental loads such as wind, current and wave, most of floating structures may have six degrees of freedom (6DoF), i.e. surge, sway, heave, roll, pitch and yaw. The present solver integrates a 6DoF motion module, which is capable of computing all six motion responses of a floating structure.

Two coordinate systems, shown in Figure 2, are introduced to describe the motion pattern of structures: a global coordinate system for calculating forces and defining movements, and a local coordinate system for constructing motion equations. These two coordinate systems, as well as variables defined in them, can be related to each other via the transformation matrices based on Euler angles (Carrica, et al., 2007). 6DoF motion equations can be then established with respect to the local coordinate system:

$$\begin{cases} \dot{u} = X/m + vr - wq + x_g(q^2 + r^2) - y_g(pq - \dot{r}) - z_g(pr + \dot{q}) \\ \dot{v} = Y/m + wp - ur + y_g(r^2 + p^2) - z_g(qr - \dot{p}) - x_g(qp + \dot{r}) \\ \dot{w} = Z/m + uq - vp + z_g(p^2 + q^2) - x_g(rp - \dot{q}) - y_g(rp + \dot{p}) \\ \dot{p} = \frac{1}{I_x} \{K - (I_z - I_y)qr - m[y_g(\dot{w} - uq + vp) - z_g(\dot{v} - wp + ur)]\} \\ \dot{q} = \frac{1}{I_y} \{M - (I_x - I_z)rp - m[z_g(\dot{u} - vr + wq) - x_g(\dot{w} - uq + vp)]\} \\ \dot{r} = \frac{1}{I_z} \{N - (I_y - I_x)pq - m[x_g(\dot{v} - wp + ur) - y_g(\dot{u} - vr + wq)]\} \end{cases} \quad (10)$$

Where m is the mass of the structure; I_x , I_y and I_z are moments of inertia around three axes of the local coordinate system; u , v and w are three components of translational velocity vector, and the dot above a variable means its time derivative, namely acceleration; p , q and r represent angular velocity vector; x_g , y_g and z_g are the coordinates of center of gravity; X , Y , Z , K , M and N represent the forces and moments, which consist of sea loads and mooring loads, and can be transformed to local coordinate system from its global counterpart.

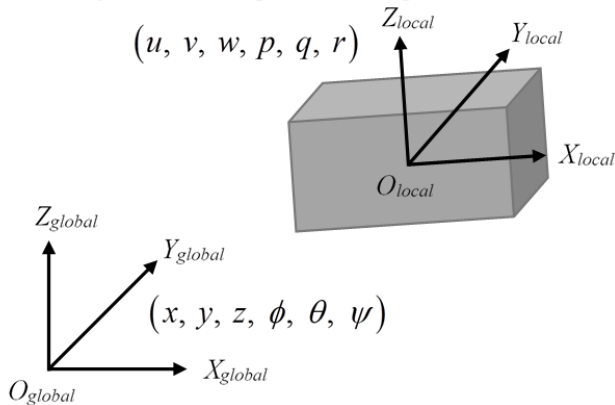


Figure 2 Definition of coordinate systems for 6DoF motion of a floating structure

The mid-rectangle formula is first adopted to compute both translational and rotational velocities in the local coordinate system, which are transformed to the global coordinate system afterwards. Linear and angular displacements are integrated again with the help of same formula. Several loops are executed before final convergence is achieved to ensure good accuracy.

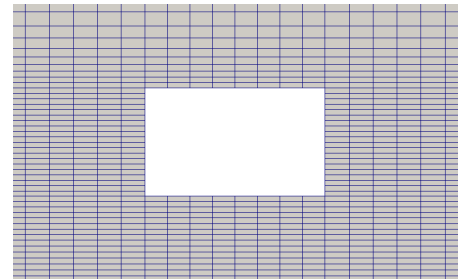
6. Dynamic mesh deformation

Once structure motion is calculated, the overall computational mesh is updated to manifest the impact of its new position on fluid field, which is achieved by employing dynamic mesh deformation technique. When the structure moves, neither the number of grid points nor the topology of grid cells changes. Instead, shape of cells transform in ways such as stretch, squeeze, translation and rotation through movement of grid points, as shown in Figure 3. Displacement of grid points \mathbf{X}_g is obtained via solving the following Laplace equation (Jasak and Tukovic, 2006):

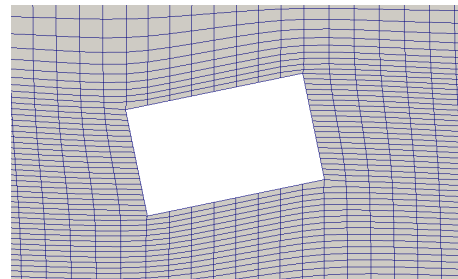
$$\nabla \cdot (\gamma \nabla \mathbf{X}_g) = 0 \quad (11)$$

Where γ represents the deformation coefficient, equal to the inverse square of the distance r from cell centers to boundaries of the structure:

$$\gamma = \frac{1}{r^2} \quad (12)$$



(a) Before deformation



(b) After deformation

Figure 3 Sketch of dynamic mesh deformation

7. Mooring system

To study the interaction problem of mooring line and floating structure, we further developed mooring system modeling methods in our existing code. It is well known that based on whether the motion of mooring lines is taken into account, general methods for solving mooring lines could be categorized as static and dynamic methods. Static analysis is always used to study static performance of mooring lines, while dynamic analysis is often adopted to calculate dynamic loading of lines which must be considered for design. In the present solver, a mooring system module containing both static and dynamic analysis methods is developed to meet diverse demands.

The piecewise extrapolating method (Hao and Teng, 2003; Fan, et al., 2012) is implemented for calculating the statics of mooring lines because it could take into account line elongation as well as the drag force induced by fluid. Multi-component lines consisting of several sections with different material characteristics can also be handled easily. With this method, mooring lines are divided into a number of segments, and a typical example of these is shown in Figure 4. Equations of static equilibrium are established in both horizontal and vertical directions:

$$\begin{cases} T_{xi+1} = T_{xi} + F_i ds \cos \varphi_{i+1} + D_i ds \sin \varphi_{i+1} \\ T_{zi+1} + D_i ds \cos \varphi_{i+1} = T_{zi} + F_i ds \sin \varphi_{i+1} + w_i dl \end{cases} \quad (13)$$

where T_x , T_z and φ represent horizontal and vertical components of tension at a cross section of one segment and the angle between tension and T_x ; dl and ds are length of the segment before and after elongation respectively; w is net submerged weight of lines per unit length; D and F denote normal and tangential components of drag force acting on the segment which are calculated using Morison's equation.

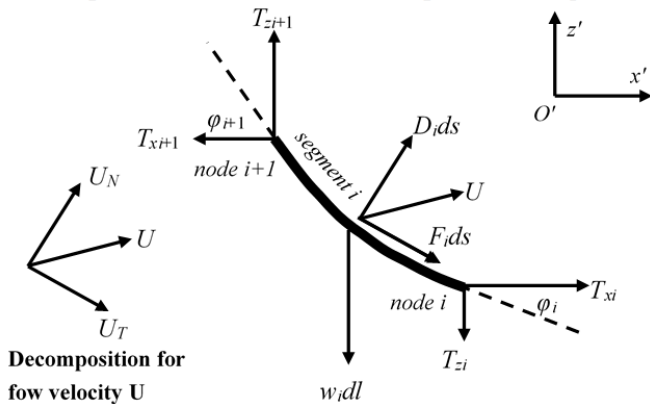


Figure 4 Force analysis of a mooring line segment for piecewise extrapolating method

For dynamic analysis, a three-dimensional lumped mass method (Huang, 1994) is developed. This method employs a spring-mass model, which discretizes a continuous line into $N+1$ point masses (nodes) connected by N massless

springs (segments) as shown in Figure 5. Considering acceleration, the dynamic equilibrium equation is built on nodes which is illustrated in Figure 6:

$$M_i \vec{a}_i = \vec{F}_{Ti} - \vec{F}_{Ti-1} + \vec{F}_{Di} + \vec{F}_{Ai} - \vec{W}_i \quad (14)$$

Where M_i and \vec{a}_i are mass and acceleration vector of node i respectively; \vec{F}_{Ti} and \vec{F}_{Ti-1} are tension vectors of segments connected by node i ; \vec{F}_{Di} and \vec{F}_{Ai} are drag and inertia forces distributed to node i from adjacent segments i and $i-1$ via averaging, which are calculated using Morison's equation as well; \vec{W}_i is gravity of node i also obtained by means of averaging. The solving procedure is similar to the one proposed by Nakajima, et al. (1982).

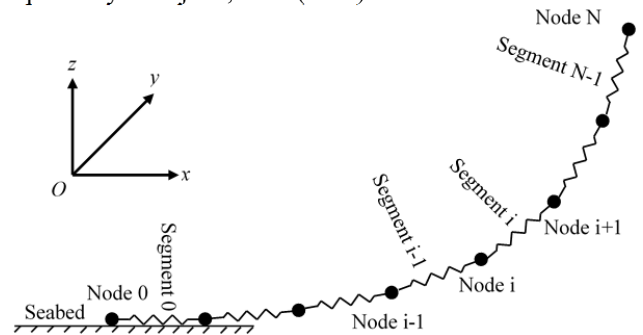


Figure 5 Sketch of spring-mass model for lumped mass method

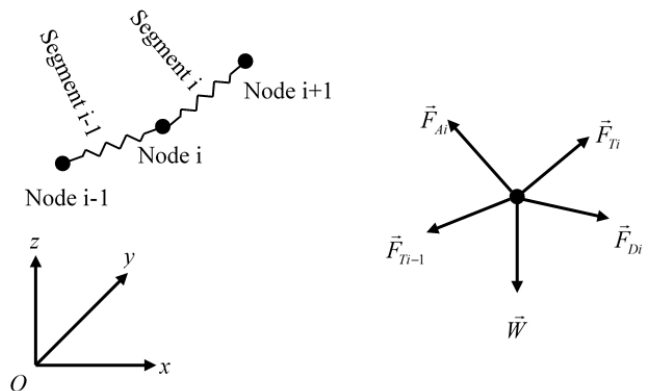


Figure 6 Force analysis of a node for lumped mass method

COMPUTATIONAL MODEL

A deep-water semi-submersible drilling platform with a catenary mooring system is selected in this study, which was investigated both experimentally and numerically by Shi (2011). Parameters of the platform and mooring system are presented in Sections 1 and 2, as well as the computational domain used to carry out numerical simulations (Section 3).

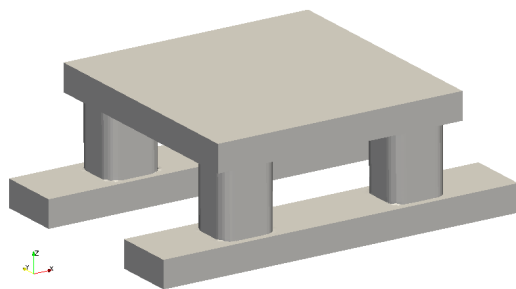
1. Platform parameters

The platform mainly consists of three parts as shown in Figure 7: a deck, four columns and two pontoons. The platform

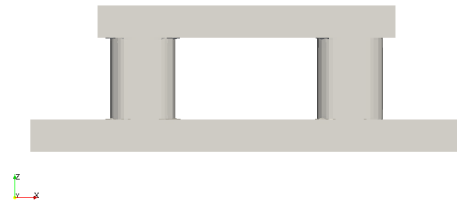
is symmetric with respect to both longitudinal and transverse sections at center plane. Primary parameters of the platform are listed in Table 1.

Table 1 Primary parameters of a deep-water semi-submersible drilling platform

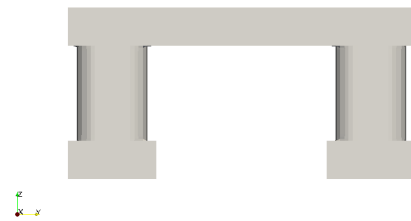
Primary parameters	Unit	Value
Deck	m	78.68×78.68×8.60
Bottom of deck above baseline	m	30.0
Column	m	17.385×15.86×21.46
Fillet radius of column	m	3.96
Longitudinal distance between centerlines of columns	m	54.83
Transverse distance between centerlines of columns	m	58.56
Pontoon	m	114.07×20.12×8.54
Distance between centerlines of pontoons	m	58.56
Tonnage	t	51465.3
Center of gravity above baseline	m	24.26
Initial air gap	m	11.0
Draft	m	19.0
Roll gyration radius	m	33.3
Pitch gyration radius	m	32.4



(a) Three dimensional model



(b) Front view



(c) Side view

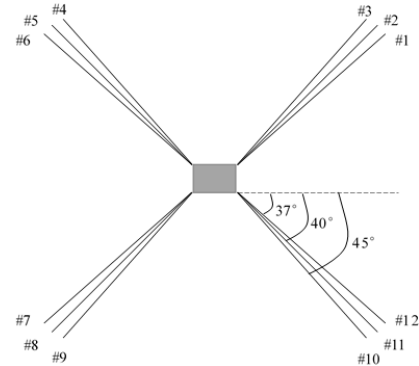


(d) Top view

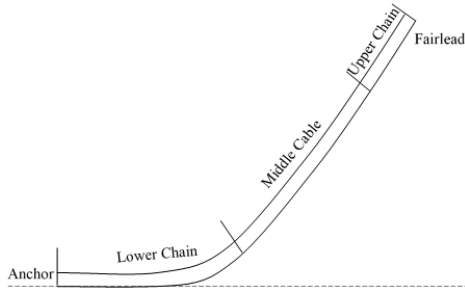
Figure 7 Sketch of a deep-water semi-submersible drilling platform

2. Mooring system configuration

The mooring system is composed of 12 lines which are symmetrically arranged into 4 groups. Numbering and angles between lines and X axis are shown in Figure 8 (a). Fairleads of all lines are positioned at the outside surface of columns.



(a) Top view



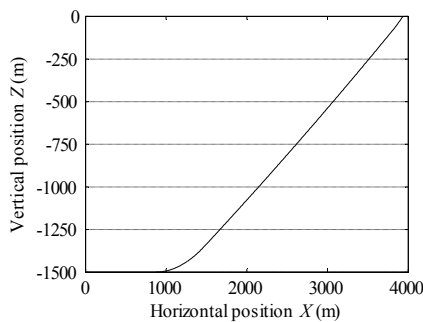
(b) Composition of a mooring line

Figure 8 Layout of mooring system for the deep-water semi-submersible platform

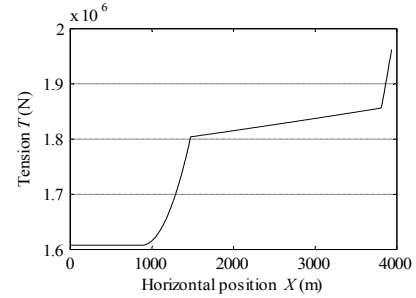
All 12 lines share same parameters. Each line is 4300m long, and made up of multi-component material which is connected by three parts with different length and material properties: the upper and lower parts are R4S chains while the middle part is polyester fiber cable, as in Figure 8 (b). Since the water depth is 1,500m, the lines exhibit catenary shape. The pretension acted on each line is 200t. Main properties of a multi-component mooring line are listed in Table 2. At the initial state, the shape and tension distribution of such a mooring line are plotted in Figure 9.

Table 2 Main properties of a multi-component mooring line

Position	Upper	Middle	Lower
Material	R4S Chain	Polyester Fiber Cable	R4S Chain
Length (m)	150	2650	1500
Diameter (mm)	84	160	84
Young's Modulus (Pa)	4.47756×10^{11}	4.67916×10^{10}	4.47756×10^{11}
Weight in Water (N/m)	1313.2	41.2	1313.2
Breaking Stress (kN)	7989	8114	7989



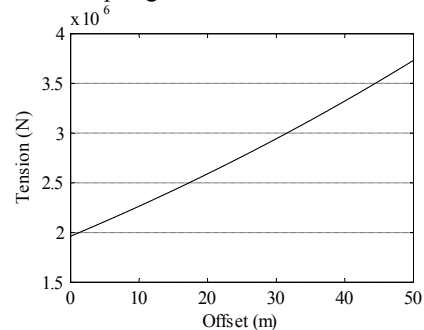
(a) Shape of mooring line



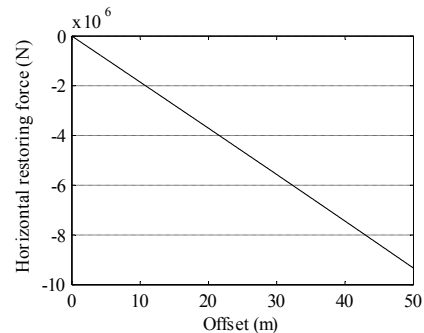
(b) Tension distribution of mooring line

Figure 9 Characteristics of mooring line at the initial state

In order to obtain the static characteristics of single mooring line, the static analysis method is employed to solve the shape and line tension at each time step when the fairlead of line moves away from the anchor horizontally at constant speed of 1m/s. Figure 10 (a) demonstrates the tension variation at the fairlead with respect to its offset. When the translational movement applies to all fairleads of the mooring system, horizontal restoring force provided by the system is obtained and plotted in Figure 10 (b). Slopes of both curves almost remains constant, revealing that the mooring system behaves much like a linear spring within offset of 50m.



(a) Tension at fairlead of single mooring line with respect to its offset



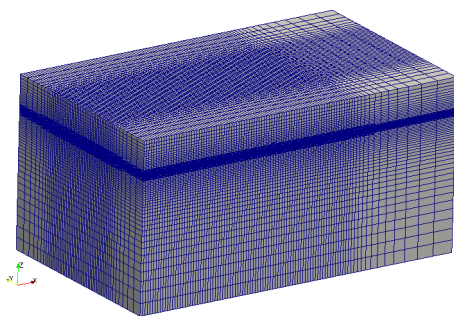
(b) Horizontal restoring force of mooring system with respect to offset

Figure 10 Static characteristics of mooring system

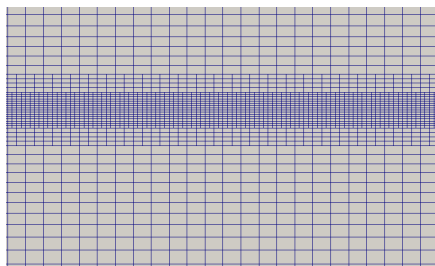
3. Computational domain

OpenFOAM provides users with a very powerful yet easy to use utility called snappyHexMesh to help create

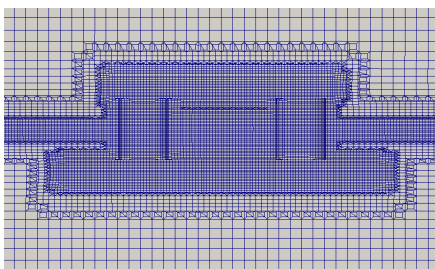
computational mesh with high quality in relatively short time. Detailed information can be found online (OpenFOAM, 2013; Silva, et al., 2010). In Figure 11 (a), mesh distribution is plotted for overall computational domain. As seen from the figure, a rectangular numerical tank is used with its dimensions as $L[-225\text{m}, 275\text{m}] \times W[-150\text{m}, 150\text{m}] \times H[-200\text{m}, 50\text{m}]$. The computational model is located at the tank center. Since the fluid field near free surface and the platform varies rather violently, cells are split locally two or more times denser than other areas to improve modeling accuracy as shown in Figure 11 (b) and (c). The ultimate cell number reaches up to nearly two million.



(a) Overview of computational mesh



(b) Local refinement near free surface



(c) Local refinement near the platform

Figure 11 Global and local view of computational mesh

VALIDATION

Under development over several years, the present solver has been used to study the problems of ship hydrodynamics and offshore engineering in various situations. Among them are wave generation and damping (Cha and Wan, 2011; Cao and

Wan, 2014), wave run-up and impacts on fixed structures (Cao, et al., 2011a; Cao, et al., 2011b; Zhou, et al., 2013), ship hydrodynamics and added resistance (Shen, et al., 2011; Ye, et al., 2012; Shen and Wan, 2013), motion response of moored floating platforms (Cao, et al., 2013; Liu, et al., 2013) and also sloshing (Shen and Wan, 2012). To validate the numerical method developed for modeling mooring system, simulated results on the dynamic response for a floating platform are compared with both experimental and numerical results from Shi (2011).

1. Incident wave

Three types of regular incident wave are chosen from previous model tests for present validation, parameters of which are listed in Table 3. Although the water is 1,500m deep under real sea states while the depth of the computational domain is merely 200m as mentioned in section 3 of the chapter *computational model*, requirements for deep water wave are satisfied if the wave length is less than twice the modeled water depth.

Table 3 Parameters of incident waves

Parameters/No.	1	2	3
Wave height (m)		6	
Wave period (s)	11.5	13	15.5
Wave length (m)	206.481	263.823	374.197

To validate whether the incident wave is well captured, a smaller domain is selected by shortening the width to $[-1\text{m}, 1\text{m}]$. As only one layer of cells is arranged in the spanwise direction, 2D simulation is performed. Take the first type of wave as an example, the curve of wave elevation at $X=-40\text{m}$ is plotted in Figure 12. It is shown that the wave changes regularly after about 6 cycles with an amplitude of 6m as prescribed, and thus the accuracy of our method is satisfactory.

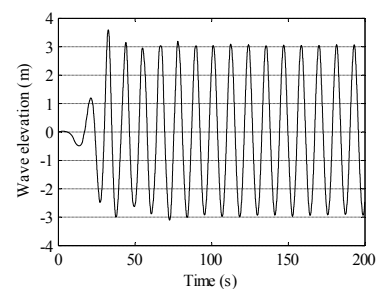


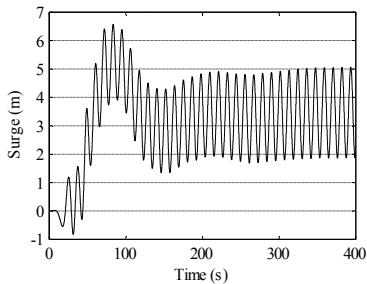
Figure 12 Wave elevation of incident wave of period $T = 11.5\text{s}$ at $X = -40\text{m}$

2. Motion responses of platform

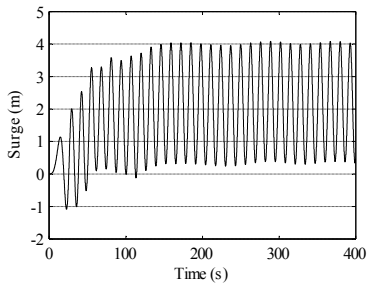
Three numerical tests are set up associated with the above mentioned three types of incident waves for validation. Incident

wave propagates in longitudinal direction of the platform, and thus only three degrees of freedom are considered, i.e. surge, heave and pitch. Lumped mass method is employed to solve the mooring system equations. The time step used is fixed at 0.02s and the overall time simulated is set as 400s.

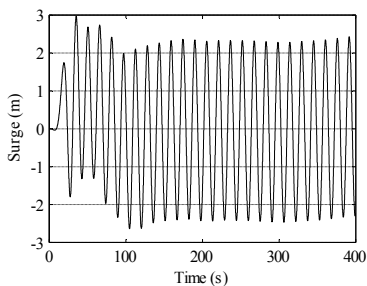
Figure 13, Figure 14 and Figure 15 show surge, heave and pitch responses of the platform within different wave periods. For comparison on Response Amplitude Operator (RAO), the results from previous numerical and experimental work are included. According to the recommendation provided by the International Towing Tank Conference (ITTC, 2002), motion data should be collected at least for 10 quasi-steady cycles under regular wave conditions to ensure accuracy of results. In this paper, time series of 200s-400s are extracted from the response curves to calculate RAO. During this time span, there are 17, 15 and 13 respectively for the three incident waves, which conforms to the recommended procedure.



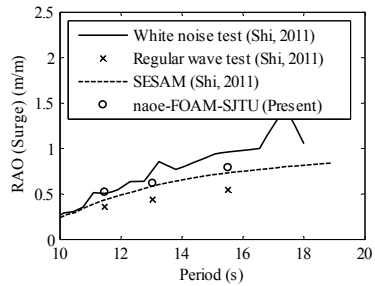
(a) Period = 11.5s



(b) Period = 13s

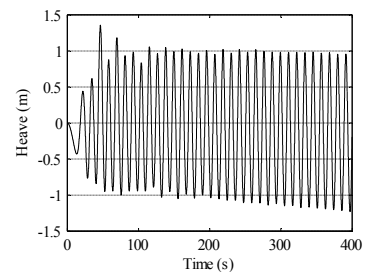


(c) Period = 15.5s

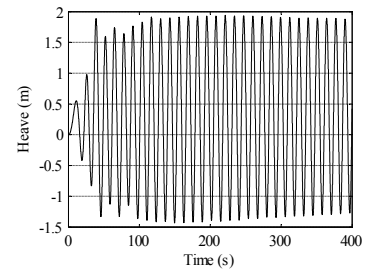


(d) Comparison of RAO

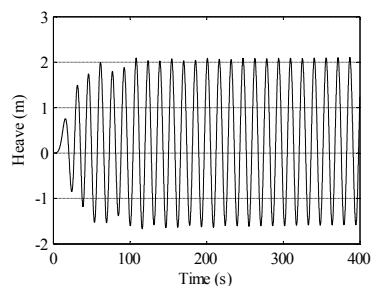
Figure 13 Results of surge response for the platform within different wave periods



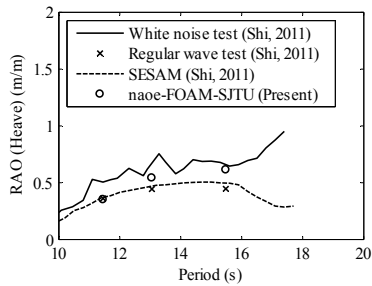
(a) Period = 11.5s



(b) Period = 13s

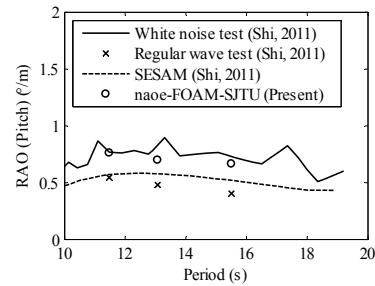


(c) Period = 15.5s



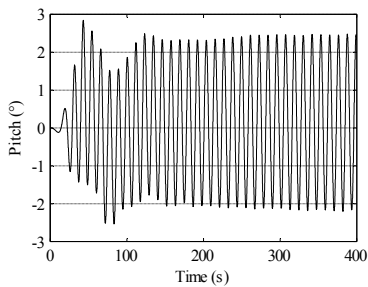
(d) Comparison of RAO

Figure 14 Results of heave response for the platform within different wave periods

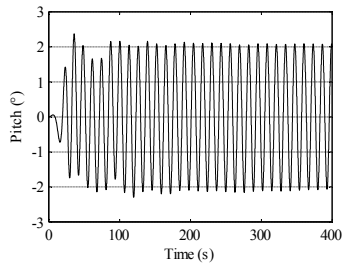


(d) Comparison of RAO

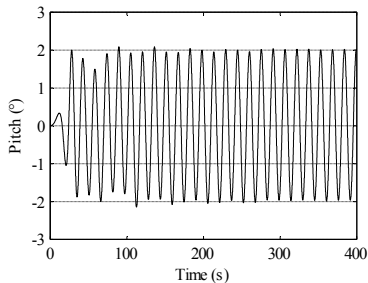
Figure 15 Results of pitch response for the platform within different wave periods



(a) Period = 11.5s



(b) Period = 13s



(c) Period = 15.5s

The comparison shows that results from various means share the same trend that RAO of surge and heave response decreases as the period of incident wave increases, while that of pitch response shows an opposite trend. Besides, results from white noise tests are larger than those of regular wave tests while present results, as well as those from SESAME, always stay between them. It could be then concluded that the present solver is capable of handling motion response problems of moored floating structures in waves. Further analysis shows that surge response of the platform becomes monochromatic after initial developing cycles, but the mean position deviates from the initial state and moves along the wave propagation direction, probably due to the drift force from wave. In addition, for working conditions discussed in this paper, the offset becomes smaller as incident wave period increases.

NUMERICAL RESULTS

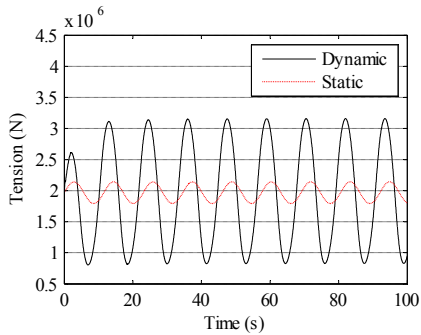
In order to evaluate the influence of mooring system parameters on the motion responses of platform, following two aspects are investigated:

- (1) different analysis methods for solving mooring lines, specifically piecewise extrapolating method for static analysis and lumped mass method for dynamic analysis (Section 1);
- (2) different mooring line compositions, i.e. varying length of each part of mooring line while keeping the overall length as a constant (Section 2);

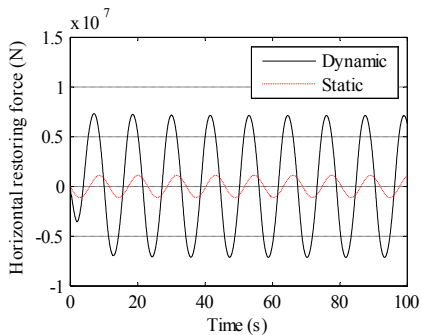
1. Effects of dynamic loading

It is well known that an important difference between static and dynamic analysis methods for solving mooring lines is whether dynamic loading is taken into account. To better illustrate the difference between two methods, movement of fairleads is specified as $x(t) = A \sin\left(\frac{2\pi}{T} \times t\right)$, where the amplitude of the movement is $A = 6m$ and the period is $T = 11.5s$. Results are depicted in Figure 16, from which it can be seen that the tension amplitude at the fairlead of a single

line obtained by dynamic analysis is almost six times larger than that from static analysis. Same trend also applies to the horizontal restoring force of the mooring system. Therefore, the static analysis method is rather conservative compared to the dynamic one. This is because dynamic loading accounts for a much larger part of overall loading and thus cannot be overlooked. In the following sections, we perform a study on whether this dynamic loading exerts large influence on the platform motion response.



(a) Tension at fairlead of a single mooring line with respect to time

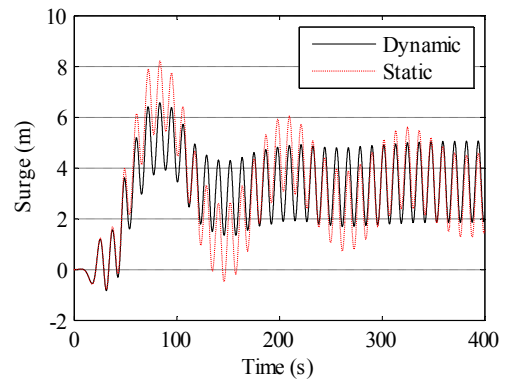


(b) Horizontal restoring force of mooring system with respect to time

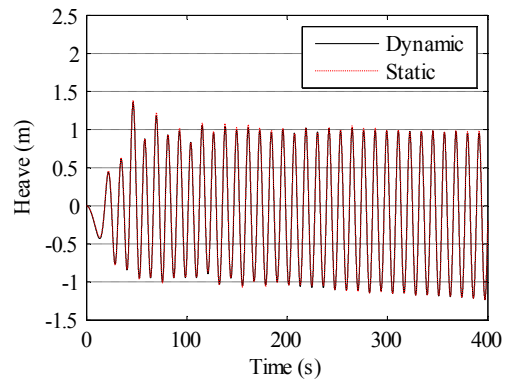
Figure 16 Comparison of characteristics of mooring system between different analysis methods

1.1 Surge, heave and pitch responses of platform

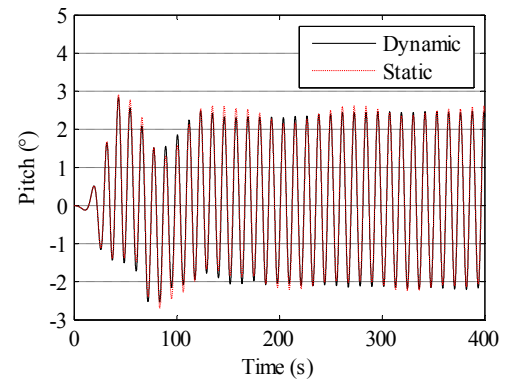
The first type of incident wave listed in Table 3 is selected as a typical case for the following simulations. Time histories of three motion responses (surge, heave and pitch) are drawn in Figure 17 to assess the results obtained from static and dynamic methods.



(a) Surge motion



(b) Heave motion



(c) Pitch motion

Figure 17 Comparison of platform responses with mooring system solved by different methods

It can be seen from Figure 17 that there is only minor discrepancy for heave and pitch responses between these two methods. Both of them present one dominant frequency as the prescribed motion. However, for surge response, apart from one frequency which corresponds to wave frequency response, results show that another low frequency with large amplitude

exists, which is induced by wave drift force. The amplitude of such low frequency response decays gradually due to damping effect. Similar phenomena is found in the study of Johanning, et al. (2007). As to this low frequency response, results from static and dynamic methods exhibit apparent difference, i.e. the prediction by dynamic method decays much faster than that from static method, leaving only the wave frequency response after about 200s.

From the above observations, we can conclude that adoption of different analysis methods for mooring systems has little impact on the heave and pitch responses of a platform. However, the difference does exist when they are applied to predict low frequency response of surge motion. Damping effect is more evident if a dynamic analysis method is adopted for mooring system modeling. Since the only difference between these two cases lies in the method employed to solve mooring lines, the additional damping effect of surge response must result from the mooring system. Therefore, dynamic analysis methods can better take into consideration the damping effect of mooring systems.

1.2 Horizontal restoring force and tension of mooring system

Figure 18 shows time histories of horizontal restoring force of the mooring system achieved by two analysis methods. Dynamic method predicts a larger amplitude than that from a static method although both curves exhibit similar trends to corresponding surge responses. In addition, the time-mean position of both curves is basically the same. This is because the mean position characterizes the wave drift force acting on the platform, which does not alter much since the operating conditions are identical using either static or dynamic modeling.

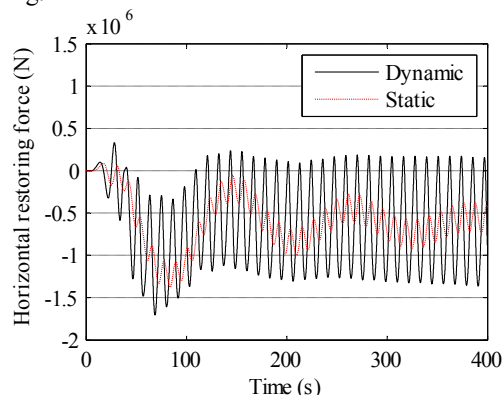
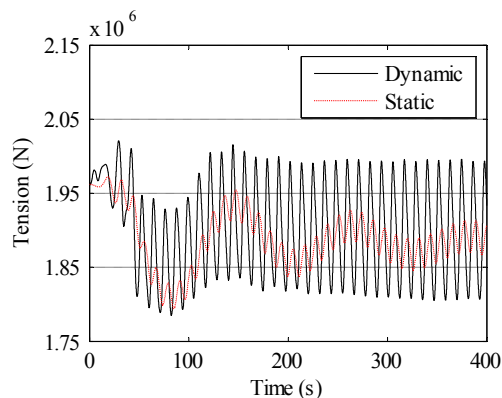
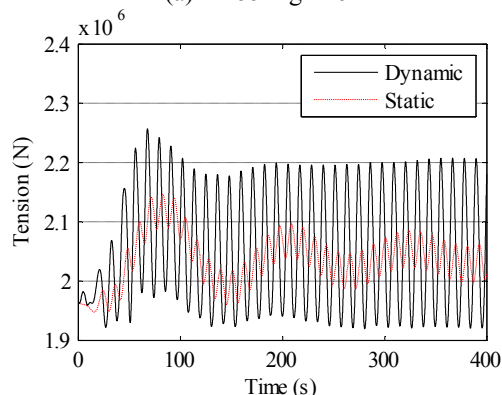


Figure 18 Horizontal restoring force of mooring system between different methods

To study the mooring line tension, two mooring lines are selected, i.e. #1 and #6 in Figure 8. Time histories of tension at fairleads of lines are drawn in Figure 19. Generally, tension of line #6 in head wave direction is larger than that of line #1 in back wave direction for both methods, because the platform shifts a bit in wave propagation direction. Moreover, for either #1 or #6, the dynamic method yields larger tension due to dynamic loading.



(a) Mooring line #1



(b) Mooring line #6

Figure 19 Tension at fairleads of mooring lines between different methods

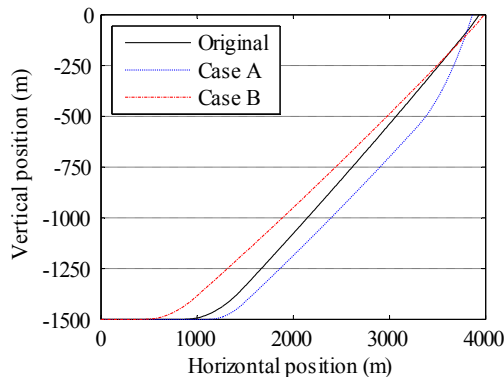
2. Effects of mooring line composition

For a multi-component mooring line, the length allocated to each part of the line can affect its shape and tension distribution. This may further exert an influence on the moored floating platform. In this section, two new configurations are set up by adjusting the length of different mooring line parts shown in Figure 8 while preserving the total length of the lines as the same as 4300m and pretension as 200t. Parameters for these three configurations are listed in Table 4.

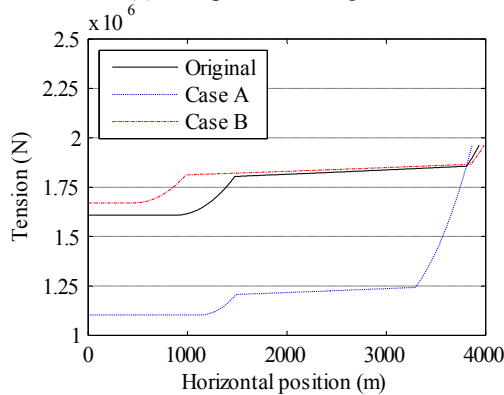
Table 4 Parameters of mooring lines with different compositions

Configurations	Original	Case A	Case B
Upper chain length (m)	150	800	150
Middle cable length (m)	2650	2000	3150
Lower chain length (m)	1500	1500	1000

Figure 20 shows the shape and tension distribution of mooring lines with three different configurations at the initial state. Variation on the mooring line composition leads to rather evident changes of shape and tension distribution of mooring lines. In terms of shape, for Case A, the three parts connect with each other un-smoothly and the grounded part of the line increases as well. The cross angle at the fairlead between the line and horizontal plane also becomes larger, indicating an increase in the vertical tension provided to the moored platform and a decrease in horizontal tension though the pretension remains the same. A reversed trend is found for Case B. In the aspect of tension distribution, tension declines at most points for Case A, especially at anchor point, where it falls from $1.60764 \times 10^6 \text{N}$ to $1.10279 \times 10^6 \text{N}$, revealing that there is less chance that the anchor can be pulled up when compared to the original case.



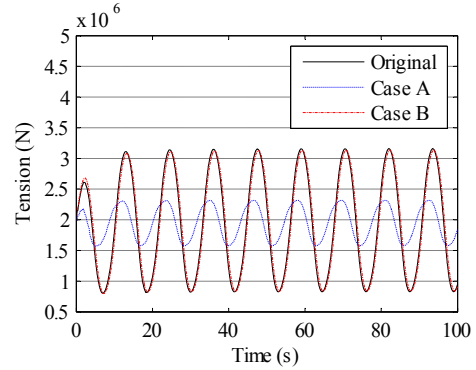
(a) Shape of mooring lines



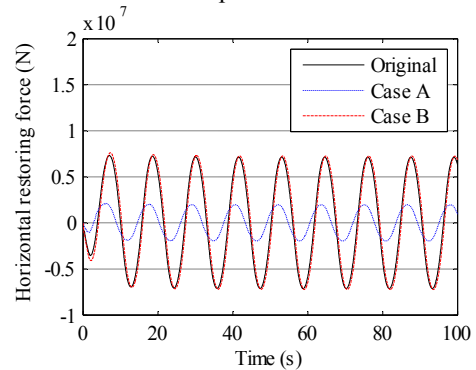
(b) Tension distribution of mooring lines

Figure 20 Initial shape and tension distribution of mooring lines with different compositions

In Figure 21 (a) and (b), the tension at fairlead of a single line and the horizontal restoring force of mooring system are displayed. Case B and the original case look very much alike while the magnitudes are reduced notably for Case A. Therefore, enlargement of middle section has little effects on the dynamic loading of mooring system, which however becomes significant if it is shortened.



(a) Tension at fairlead of a single mooring line with respect to time



(b) Horizontal restoring force of mooring system to time

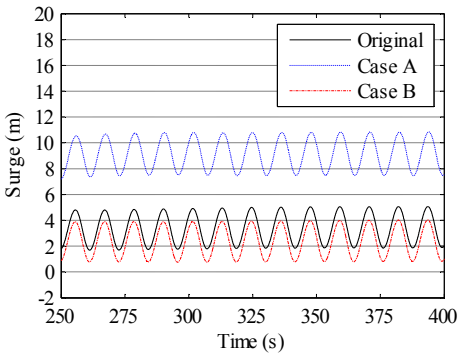
Figure 21 Comparison of characteristics of mooring system with different line compositions

2.1 Surge, heave and pitch responses of platform

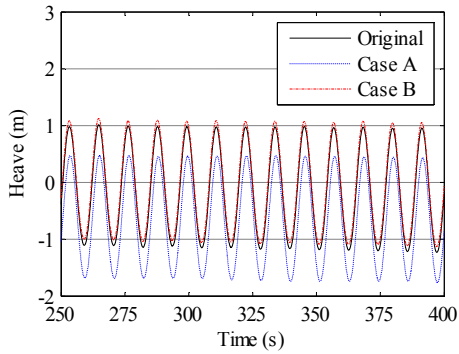
Motion responses of the two new configurations are estimated and compared to the original configuration as shown in Figure 22. Only the results between 250s and 400s are extracted to compute RAOs for three motion responses listed in Table 5. Results show that the mooring line composition has influences on 3DoF motion responses of platform though the extent to which varies.

Table 5 RAO of the platform with mooring system of different mooring line compositions

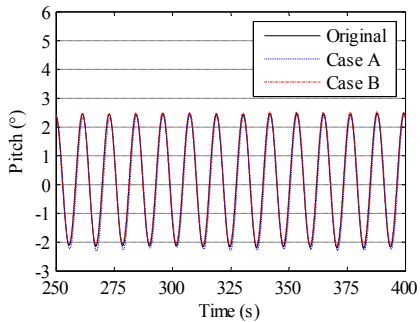
Configurations	Original	Case A	Case B
Surge RAO (m/m)	0.5205	0.5521	0.5205
Heave RAO (m/m)	0.3523	0.3604	0.3523
Pitch RAO (°/m)	0.7612	0.7716	0.7566



(a) Surge motion



(b) Heave motion



(c) Pitch motion

Figure 22 Comparison of platform responses with mooring system of different line compositions

For surge response, increasing the upper chain length leads to a larger RAO, and the mean position deviates further approaching 9m, which is caused by smaller dynamic loading. Increasing length of the middle cable part, on the other hand, does not alter the RAO, and relatively larger dynamic loading restricts drift movement a bit. For heave response, the configuration of Case A leads to a slight increase of its RAO while the mean position falls under the initial draft because the vertical component of pretension alters the floating state of the platform. On the contrary, RAO remains nearly unchanged for Case B and the mean position rises slightly due to a similar reason. For pitch response, three curves are rather close to each other and RAOs are also quite similar.

We can therefore conclude that surge response is relatively more sensitive to the mooring line composition than heave and pitch responses. Longer upper chain results in a larger surge RAO, thus aggravating motion response within the wave frequency domain. Different configurations also affect the surge response in low frequency domain. The platform drifts further when the upper chain part becomes longer. Viewed from this perspective, increasing length of the middle cable is preferable. The mean position of heave response is also influenced via vertical component of pretension, while pitch response is not much affected.

2.2 Horizontal restoring force and tension of mooring system

Figure 23 shows the time histories of horizontal restoring force of the mooring system with different mooring line compositions. Corresponding to the results drawn in Figure 21, the horizontal restoring force becomes smaller for Case A while that force for Case B is a bit larger.

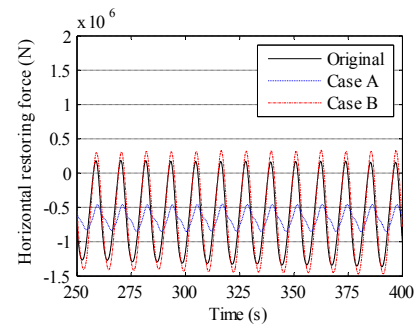
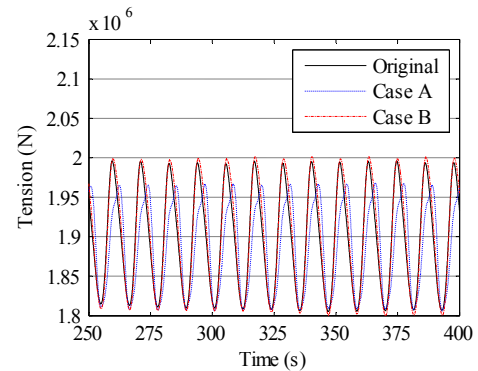
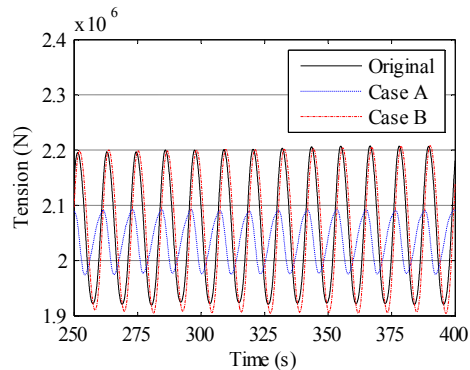


Figure 23 Horizontal restoring force of mooring system with different line compositions

Figure 24 demonstrates the time histories of tension at fairleads of mooring lines #1 and #6 with different mooring line compositions. For Case A, the maximum tension of both lines drops and that of line #6 in head wave direction decreases more. On the other hand, tension for Case B does not change much.



(a) Mooring line #1



(b) Mooring line #6

Figure 24 Tension at fairleads of mooring lines with different compositions

DISCUSSIONS

With regard to heave and pitch responses, floating structures can provide much larger hydrostatic stiffness than mooring systems. Therefore, mooring systems would have only little impact on the heave and pitch responses of floating structures. In such cases, no matter how the mooring system varies, such as they are analyzed by different methods (static and dynamics) or the system configurations change, the heave and pitch responses of the platform are almost unchanged except for the mean position of heave response influenced by the vertical component of mooring line pretension.

On the other hand, floating structures cannot provide hydrostatic stiffness to the surge response, mooring systems are thus essential and have large impacts on platform surge response. Two common surge response are wave frequency response (namely RAO) and low frequency response, which gradually damps out to a steady drift under regular wave conditions. It is noted that the mooring system influence low frequency response more than RAO. Drift motion, i.e. the mean position of wave frequency response, is determined by both the wave drift force and the horizontal restoring force of the mooring system. Under the same wave conditions, wave drift force acting on the platform remains unchanged while the platform has to drift farther if its mooring system provides less restoring force. On the other hand, damping effects are larger for dynamic than static analysis methods because the former takes into account the velocity of mooring line segments, thus resulting in larger drag force. Larger damping means that low frequency response can damp out more quickly.

Among the aforementioned three responses, mooring systems are affected mostly by surge response due to its relatively large magnitude. Horizontal restoring force of the mooring system and tension of lines are therefore closely related to the time history of surge. Larger the surge response is, larger the horizontal restoring force of the mooring system and mooring line tension are.

CONCLUSIONS

In this paper, a viscous flow solver naoe-FOAM-SJTU based on the open source toolbox OpenFOAM is developed and presented. By comparing numerically calculated results with those obtained from model tests, the ability of present solver to handle hydrodynamic problems of floating structures with mooring systems under various wave conditions is validated. The solver is then adopted to investigate the effects of mooring system on the dynamic response of a semi-submersible platform (surge, heave and pitch) with a viscous fluid condition. The horizontal restoring force of the mooring system and mooring line tension are also investigated. Two sets of numerical simulation are carried out regarding different analysis methods for solving mooring lines and different mooring line compositions. Although at current stage, the application of present solver in this paper is limited to regular wave conditions, it can be easily extended to irregular or extreme waves afterwards. The work done in this paper can serve as the foundation for our future relevant hydrodynamic studies such as slamming and green water phenomena of floating structures, as well as VIV of Spar platforms.

ACKNOWLEDGMENTS

The work is supported by National Natural Science Foundation of China (Grant Nos. 51379125, 51490675, 11432009, 51411130131), National Key Basic Research Development Plan (973 Plan) Project of China (Grant No. 2013CB036103), the Program for Professor of Special Appointment (Eastern Scholar) at Shanghai Institutions of Higher Learning (Grant No. 2013022), and Center for HPC at Shanghai Jiao Tong University, to which the authors are most grateful.

REFERENCES

- [1] Baudic, S.F., Williams, A.N., Kareem, A. A Two-Dimensional Numerical Wave Flume—Part 1: Nonlinear Wave Generation, Propagation, and Absorption[J]. *Journal of Offshore Mechanics and Arctic Engineering*. 2001, **123**(2): 70-75.
- [2] Cao, H., Liu, Y., Wan, D.C., Yang, C. Numerical simulation of solitary wave impact on fixed offshore platform. In *The 7th International Workshop on Ship Hydrodynamics*. Shanghai, China. 2011a: 138-143.
- [3] Cao, H. and Wan, D.C. Development of Multidirectional Nonlinear Numerical Wave Tank by naoe-FOAM-SJTU Solver[J]. *International Journal of Ocean System Engineering*. 2014, **4**(1): 52-59.
- [4] Cao, H., Wang, X., Liu, Y. and Wan, D.C. Numerical Prediction of Wave Loading on a Floating Platform Coupled with a Mooring System. In *The Twenty-third International Offshore and Polar Engineering Conference*. Anchorage, Alaska, USA. 2013: 582-589.
- [5] Cao, H., Zha, J. and Wan, D.C. Numerical simulation of wave run-up around a vertical cylinder. In *Proceedings of the Twenty-first (2011) International Offshore and Polar Engineering Conference*, Maui, Hawaii, USA. 2011b: 726-

- 733.
- [6] Carrica, P.M., Wilson, R.V., Noack, R.W., Stern, F. Ship motions using single-phase level set with dynamic overset grids[J]. *Computers & Fluids*. 2007, **36**(9): 1415-1433.
- [7] Cha, J. and Wan, D.C. Numerical wave generation and absorption based on OpenFOAM[J]. *The Ocean Engineering*. 2011, **29**(3): 1-12.
- [8] Diamantoulaki, I., Angelides, D.C. Modeling of cable-moored floating breakwaters connected with hinges[J]. *Engineering Structures*. 2011, **33**(5): 1536-1552.
- [9] Fan, T., Qiao, D., Ou, J. Optimized Design of Equivalent Truncated Mooring System Based On Similarity of Static And Damping Characteristics. In *The Twenty-second International Offshore and Polar Engineering Conference*. Rhodes, Greece. 2012: 959-966.
- [10] Hall, M., Buckham, B., Crawford, C., Nicoll, R.S. The importance of mooring line model fidelity in floating wind turbine simulations. In *OCEANS 2011*. Hilton Waikoloa Village, Waikoloa, HI, USA. 2011: 1-8.
- [11] Hao, C., Teng, B. Static analysis for a non-uniform flexible mooring cable system[J]. *China Offshore Platform*. 2003, **18**(4): 18-21.
- [12] Hirt, C.W., Nichols, B.D. Volume of fluid (VOF) method for the dynamics of free boundaries[J]. *Journal of Computational Physics*. 1981, **39**(1): 201-225.
- [13] Huang, S. Dynamic analysis of three-dimensional marine cables[J]. *Ocean Engineering*. 1994, **21**(6): 587-605.
- [14] ITTC. ITTC Recommended Procedures – Sea Keeping Experiments. 2002: 4.
- [15] Jasak, H., Tukovic, Z. Automatic mesh motion for the unstructured finite volume method[J]. *Transactions of FAMENA*. 2006, **30**(2): 1-20.
- [16] Jeon, S.H., Cho, Y.U., Seo, M.W., Cho, J.R., Jeong, W.B. Dynamic response of floating substructure of spar-type offshore wind turbine with catenary mooring cables[J]. *Ocean Engineering*. 2013, **72**: 356-364.
- [17] Johanning, L., Smith, G.H., Wolfram, J. Measurements of static and dynamic mooring line damping and their importance for floating WEC devices[J]. *Ocean Engineering*. 2007, **34**(14): 1918-1934.
- [18] Kim, B.W., Sung, H.G., Kim, J.H., Hong, S.Y. Comparison of linear spring and nonlinear FEM methods in dynamic coupled analysis of floating structure and mooring system[J]. *Journal of Fluids and Structures*. 2013, **42**: 205-227.
- [19] Larsen, J., Dancy, H. Open boundaries in short wave simulations—a new approach[J]. *Coastal Engineering*. 1983, **7**(3): 285-297.
- [20] Liu, Y., Sun, R., Cao, H. and Wan, D.C. Motion response analysis of a semi-submersible platform with catenary mooring system. In *Proceedings of the Eighth International Workshop on Ship Hydrodynamics*. Seoul, Korea. 2013.
- [21] Nakajima, T., Motora, S., Fujino, M. On the dynamic analysis of multi-component mooring lines. In *Offshore Technology Conference*. 1982: 105-120.
- [22] OpenFOAM. Mesh generation with the snappyHexMesh utility. 2013. Available from: <http://www.openfoam.org/docs/user/snappyHexMesh.php#x26-1510005.4>.
- [23] Qiao, D., Ou, J. Global responses analysis of a semi-submersible platform with different mooring models in South China Sea[J]. *Ships and Offshore Structures*. 2013, **8**(5): 441-456.
- [24] Rahman, M.A., Mizutani, N., Kawasaki, K. Numerical modeling of dynamic responses and mooring forces of submerged floating breakwater[J]. *Coastal Engineering*. 2006, **53**(10): 799-815.
- [25] Rusche, H. Computational Fluid Dynamics of Dispersed Two-phase Flows at High Phase Fractions. [Doctoral Dissertation]. London: University of London. 2002.
- [26] Seebai, T., Sundaravadivelu, R. Effect of Taut And Catenary Mooring On Spar Platform With 5MW Wind Turbine. In *The Eighth (2009) ISOPE Ocean Mining Symposium*. Chennai, India. 2009: 52-58.
- [27] Sethuraman, L., Venugopal, V. Hydrodynamic response of a stepped-spar floating wind turbine: Numerical modelling and tank testing[J]. *Renewable Energy*. 2013, **52**: 160-174.
- [28] Shen, Z., Cao, H., Ye, H., Liu, Y. and Wan, D.C. Development of CFD Solver for Ship and Ocean Engineering Flows. In *8th International OpenFOAM Workshop*. Jeju, Korea. 2013.
- [29] Shen, Z., Jiang, L., Miao, S., Wan, D.C., Yang, C. RANS Simulations of Benchmark Ships Based on Open Source Code. In *Proceedings of the Seventh International Workshop on Ship Hydrodynamics*. Shanghai, China. 2011: 76-82.
- [30] Shen, Z. and Wan, D.C. Numerical Simulations of Large-Amplitude Motions of KVLCC2 with Tank Liquid Sloshing in Waves. In *2nd International Conference on Violent Flows*. Nantes, France. 2012: 149-156.
- [31] Shen, Z. and Wan, D.C. RANS Computations of Added Resistance and Motions of a Ship in Head Waves[J]. *International Journal of Offshore and Polar Engineering*. 2013, **23**(4): 263-271.
- [32] Shi, Q. Research on kinetic and dynamic characteristics of a deepwater drilling semi-submersible platform. [Master's Thesis]. Shanghai, China: Shanghai Jiao Tong University. 2011. (In Chinese).
- [33] Silva, G.A.L.d., Arima, M.N., Sousa, F.D.d. Mesh Generation in OpenFoam® with SnappyHexMesh. 2010. Available from: http://www.ats4i.com.br/en/publications/files/SnappyHexMesh_1stOpenFoamBRAZIL_linux.pdf.
- [34] Sun, J.W., Fan, X.T., Wan, X.Z., Liu, S.X. Numerical Study on Hydrodynamic Behavior of Deepwater Spar Platform with Different Mooring Configurations[J]. *Applied Mechanics and Materials*. 2012, **137**: 50-58.
- [35] Tahar, A., Kim, M.H. Coupled-dynamic analysis of floating structures with polyester mooring lines[J]. *Ocean Engineering*. 2008, **35**: 1676-1685.
- [36] Waris, M.B., Ishihara, T. Influence of mooring force estimation on dynamic response of floating offshore wind turbine system. In *Renewable Energy 2010 International*

- Conference. Yokohama, Japan. 2010.
- [37] Waris, M.B., Ishihara, T. Dynamic response analysis of floating offshore wind turbine with different types of heave plates and mooring systems by using a fully nonlinear model[J]. *Coupled Systems Mechanics*. 2012, **1**(3): 247-268.
- [38] Ye, H., Shen, Z. and Wan, D.C. Numerical prediction of added resistance and vertical ship motions in regular head waves[J]. *Journal of Marine Science and Application*. 2012, **11**(4): 410-416.
- [39] Yilmaz, O., Incecik, A. Hydrodynamic design of moored floating platforms[J]. *Marine Structures*. 1996, **9**(5): 545-575.
- [40] Zha, R., He, H., Shen, Z. and Wan, D.C. Numerical Computations of Resistance of High Speed Catamaran in Calm Water. *Journal of Hydrodynamics*. 2014, **26**(6): 930-938
- [41] Zhao, W. and Wan, D.C. Numerical Study of Interactions Between Phase II of OC4 Wind Turbine and Its Semi-Submersible Floating Support System. *Journal of Ocean and Wind Energy*. 2015, **2**(1): 45-53
- [42] Zhou, H., Cao, H. and Wan, D.C. Numerical Predictions of Wave Impacts on the Supporting Structures of Shanghai Donghai-Bridge Offshore Wind Turbines. In *The Twenty-third International Offshore and Polar Engineering Conference*. Anchorage, Alaska, USA. 2013: 216-224